Peer-reviewed version available at *Appl. Sci.* **2020**, *10*, 3595; doi:10.3390/app10103595

Article

Exploiting Localized Surface Plasmon Resonances in Subwavelength Spiral Disks for THz Thin Film Sensing

Vasily V. Gerasimov [1,2]*, Ruslan R. Hafizov [1,2], Sergei A. Kuznetsov [1,2,3], and Pavel A. Lazorskiy[2,4]

[1] Budker Institute of Nuclear Physics SB RAS, 11, Ac. Lavrentiev Ave., Novosibirsk, 630090, Russia, v.v.gerasimov3@gmail.com,
[2] Novosibirsk State University, 2, Pirogov St., Novosibirsk, 630090, Russia, khrusle@gmail.com
[3] Rzhanov Institute of Semiconductor Physics SB RAS, Novosibirsk Branch "TDIAM", 2/1, Ac. Lavrentiev Ave., Novosibirsk, 630090, Russia, sakuznetsov@nsm.nsu.ru
[4] Institute of Laser Physics SB RAS, 11, Ac. Lavrentiev Ave., Novosibirsk, 630090, Russia, pavellasor@ya.ru
* Vasily Gerasimov: v.v.gerasimov3@gmail.com; Tel.: +7-383-3294839

Abstract: In this paper, we study the sensing performance of metasurfaces comprised by spiral-disk-shaped metallic elements patterned on polypropylene substrates, which exhibit localized surface plasmon resonances in the low-frequency region of the THz spectrum (0.2-0.5 THz). Optimal designs of spiral disks with C-shaped resonators placed near the disks were determined and fabricated. The experimentally measured transmittance spectra of samples coated with very thin photoresistive layers ($d \sim 10^{-4}$-10^{-3} λ) showed good agreement with simulations. The resonance frequency shift Δf increases with increasing d, while saturating near $d = 50$ μm. The narrow-band magnetic dark modes excited on symmetrical spiral disks with a 90^0-C-resonator demonstrated very high FOM values reaching 1670 $[\text{RIU}\cdot\text{mm}]^{-1}$ at 0.3μm-thick analyte. The hybrid high order resonances excited on asymmetrical densely packed spiral disks showed about two times larger FOM values (up to 2950 $[\text{RIU}\cdot\text{mm}]^{-1}$) as compared to symmetrical distantly spaced spirals that resembles the best FOM results found in literature for metasurfaces fabricated with a similar technique. The demonstrated high sensing performance of spiral disks is evaluated to be promising for bio-sensing applications in the THz range.

Keywords: metasurface; localized surface plasmon resonance; thin-film sensor; terahertz.

1. Introduction

Localized plasmon resonance (LPR) is resonant oscillation of the charge density of free electrons in conducting particles of sub-wavelength size in an oscillating external field, accompanied by enhancement of the near field at the surface of the particles [1]. LPRs exhibit strong spatial localization and amplification of electromagnetic field near the particle surface with the resonance frequency depending on the shape, size, and conductivity of the particle and its environment. These properties have wide applications in the visible frequency range: in chemical sensors and biosensors [2], surface-enhanced Raman spectroscopy [3], fluorescence amplification [4], second harmonic generation [5], solar cells [6], and photocatalysis [7].

The terahertz (THz) spectral range (covering the frequency domain from 0.1 to 10 THz) is of great importance for biology due to nonionizing nature of THz waves and the fact that rotational and vibrational modes of complex intra- and extra-molecule bonds of many important chemical and biological substances lie in this region [8-10]. This explains high prospects of using plasmon resonances in the THz range for sensing and spectroscopy. It is worth noting, however, that the THz frequencies ($\omega_{THz} \sim 10^{12}$ Hz) are several orders of magnitude lower than the plasma frequency of free electrons in metal ($\omega_p \sim 10^{16}$ Hz) and their collision frequency ($\omega_c \sim 10^{14}$ Hz [11]), and, therefore,

plasmon resonances formally cannot be excited in this spectral region. To overcome these limitations, Pendry and his colleagues suggested making periodic corrugation of flat surface [12] that leads to forming bound surface states with high confinement of electromagnetic field, so called "spoof surface plasmon resonances". It has been shown that sub-wavelength metallic structures [13] are able to support spoof localized surface plasmon resonances (LSPRs) in the long-wave region. This idea was elaborated in detail in the metamaterial community through the concept of plasmonic metasurfaces (PMSs) [14, 15], which are understood as thin metallic screens with periodically patterned subwavelength apertures or substrate-backed arrays of subwavelength metallic elements. It is essential that LSPRs excited on a PMS are directly related to geometry of the PMS unit cells that provides high flexibility in engineering EM properties of the structures both in far and near field. Alongside with feasibility of versatile frequency selective and polarization transforming devices, this approach enables creating high-performance PMS-based sensors of thin-film analytes. Exploiting the LSPR-induced effect of near-field confinement, which enhances light–matter interaction, such sensors exhibit high sensitivity to dielectric environment and allow determining analytes with thicknesses several orders of magnitudes smaller than the LSPR wavelength via tracking a frequency shift of the LSPR relative to that of a bare PMS (without a deposited analyte).

Applicable to THz, a comprehensive review of thin film sensing with metasurfaces is given in [16]. From a technological viewpoint, the THz range is attractive due to its relatively large (compared to VIS and IR domains) wavelengths as it allows one to use well-mastered and inexpensive micromachining technologies, such as photolithography, in the PMS fabrication. Furthermore, the Ohmic losses in metal and dielectric losses in substrates, that serve as an obstacle at shorter wavelengths, does not play such a crucial role at THz frequencies and can be neglected in many cases. Plasmon resonances with lower losses have higher *Q*-factors that facilitates high-sensitivity sample detection via precise measurement of small resonant shifts. In this work, we propose using PMSs with spiral-disk-shaped metallic elements patterned on low-loss polypropylene substrates for THz sensing of thin dielectric films.

For the first time, a design of the LSPR-structure with azimuthally patterned (grooved) metal disks (see Figure 1(a)) was proposed and studied in the microwave region [13,17]. The grooves were filled with a dielectric material and the surrounding medium was air. For efficient confinement of the surface mode on the structure, the period of grooves at the outer radius R must be much less than the radiation wavelength in air: $G = 2\pi R/N << \lambda_0$, where N is a total number of grooves. Lately, numerical simulations in the THz region for a periodic structure of azimuthally grooved golden disks on dielectric substrates [18-21] showed that high order (multipole) electric and magnetic LSPRs can be excited under oblique illumination or when combining the grooved disk with a C-shaped resonator. As compared to dipole resonances, the multipole ones have higher *Q*-factors and are more sensitive to the presence of dielectric materials on the structure, i.e. more promising for sensing applications.

An azimuthally grooved disk supports the resonances up to the asymptotic frequency f_a, which depends on the groove width h and the refractive index n in the groove as $f_a = c/(4h \cdot n)$, where c is the light speed [22]. Increase in the width h shifts the asymptote frequency (and the resonance spectrum) towards lower frequencies and, consequently, enhances confinement of LSPR modes. Thus, the lowest resonant frequency is governed by the size of the disk. To improve the mode confinement of spoof LSPRs, it was suggested to use long spiral grooves (Figure 1(b)) [23]. Extension of spirals allows shifting the LSPR resonances towards longer wavelengths, exceeding by far the structure size, that yields stronger EM field localization near the surface. Thus, a spiral disk design is expected to be very promising for sensing applications at THz, whereat this kind of structures is still understudied. It is worth mentioning that numerical calculations, theoretical analysis, and experimental tests of spiral grooves were reported in literature mainly for the microwave region [22], and we know only one paper on experimental implementation of a simple design of spiral disks in the THz range [24].

Preprints (www.preprints.org) | NOT PEER-REVIEWED | Posted: 23 April 2020 doi:10.20944/preprints202004.0408.v1

Peer-reviewed version available at Appl. Sci. 2020, 10, 3595; doi:10.3390/app10103595

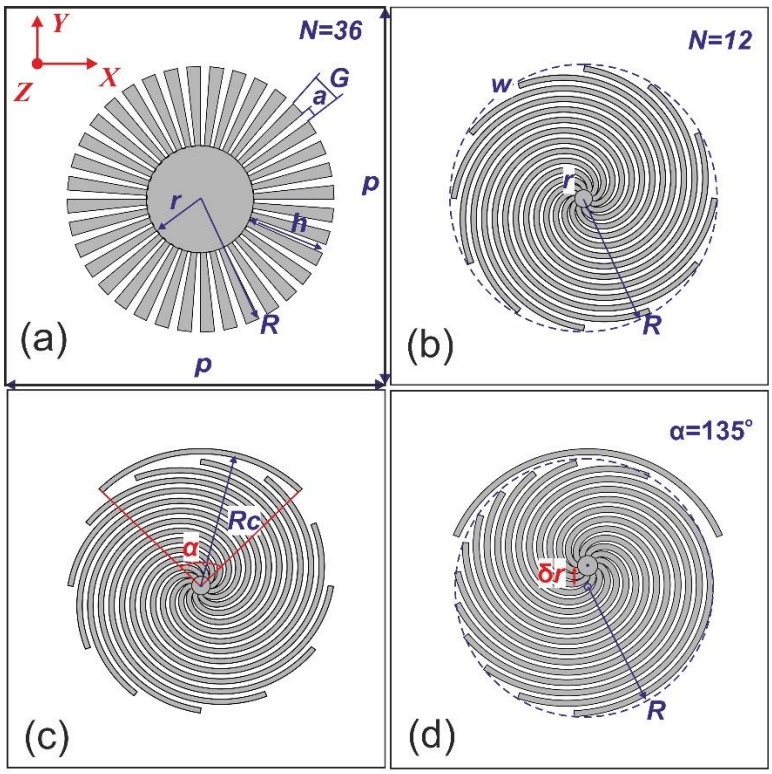

Figure 1. Four different designs of PMSs with metal disk elements (unit cells are shown; p is lattice constant): (**a**) azimuthally patterned disk; (**b**) spiral disk; (**c**) spiral disk with C-shaped resonator (α is resonator's arch angle); (**d**) spiral disk with C-shaped resonator and shifted center (δr is center shift).

In this paper, we present the results of numerical simulations and experimental testing of spiral metal disks patterned on a dielectric substrate to excite electric and magnetic multipole LSPRs in the spectral region of 0.2–0.5 THz. The packing density of the disks in the array, addition of a C-shaped resonator, asymmetric design of the spirals, and oblique illumination are studied. Testing of the optimal designs shows that spiral metal disks are very promising for THz sensing of thin-film analytes.

2. Materials and Methods

Figure 1(b-d) presents schematic drawings of Archimedes spiral disk designs under study. Using the investigation results for similar structures in the microwave region [22] and taking into account our technological limitations, we rescaled spiral disk parameters to the range of 0.2–0.5 THz compatible with our instrumentation capabilities: the inner radius r = 18 μm, the outer radius R = 192 μm, the spiral arm line width w = 8 μm, the number of arms N = 12. We considered two types of arrays differed in the lateral periodicity p of single spirals in the X- and Y-directions: 1) p = 768 μm, distantly spaced disks; 2) p = 408 μm, closely spaced disks with a "hybridization effect" (excitation of hybridized plasmon modes).

The transmittance spectra of a periodic array of spiral disks in the range of 0.2–0.5 THz were simulated using commercial CST Microwave Studio Suite software, wherein the regime of Floquet ports and periodic boundary conditions applied to the structure's unit cell was employed. In this regime, oblique illumination of the structure was modeled through specifying the orientation angles (θ, φ) of the incident wave vector $\boldsymbol{k}$ in the XYZ coordinate system: the polar angle θ describes the angle between $\boldsymbol{k}$ and Z-axis, while the azimuthal angle φ defines the angle between the orthogonal projection of $\boldsymbol{k}$ on the XY plane measured from the X-direction. Since a THz beam was horizontally polarized in our experiments and a rotary stage afforded rotation of the sample only around a vertical axis, our investigations were limited by TM-polarized excitation. Two marginal cases were considered: $\varphi = 0$ and $\varphi = 90°$. The former is of primary importance since it enables proper excitation of the C-shaped resonator ($\boldsymbol{E}_{in\text{-}plane} \parallel X$), as elucidated in Section 3.1.

The spirals were modeled as 0.35μm-thick aluminum layers with dispersionless conductivity $\sigma = 1.5*10^7$ S/m [25,26] placed on top of a 15μm-thick polypropylene (PP) film with the dielectric permittivity $\varepsilon_{PP} = 2.25 \cdot (1 - j \cdot 10^{-3})$ [25,26]. PP has low absorption in the THz range and was intentionally chosen as a substrate material to minimize the dielectric losses in the structure; we also used the thinnest PP substrate available to diminish interference effects in the PP layer.

The designed structures were fabricated with a standard contact photolithography technique, which was specifically adapted for operations on flexible polymeric substrates [26-28]. Each 15-μm-PP film sample was carefully tightened onto a bearing Al ring with a clear aperture diameter of 3 inches which specified the optical diameter of the output PMS. Al metallization was sputtered onto the PP films by means of a vacuum thermal deposition method. Prior to sputtering, the PP substrates were treated with a glow discharge in O_2 atmosphere to improve adhesion of Al to PP.

The sensing performance of the structure was tested by depositing a photoresistive material (AR-P 3250 produced by ALLRESIST GmbH [29]) of variable thickness (from 0.3 to 10 μm) on the PP film using a standard spin coating deposition technique. The photoresist was considered as a nondispersive and lossless analyte with $\varepsilon_a = 2.65$ ($n_a \approx 1.63$), experimentally evaluated in the spectral range considered [30].

To measure the complex transmission coefficient of the fabricated samples in the range of 230–540 GHz, a sub-terahertz quasi-optical backward wave oscillator (BWO) spectrometer developed in the Prokhorov General Physics Institute RAS (Moscow, Russia) [31] was used. This frequency-domain (continuous-wave, CW) instrument is equipped with a Golay cell to detect the THz signal and exploits the arrangement of the dual-path polarizing Mach-Zehnder interferometer for phase-sensitive measurements [32]. We employed a classical scheme with a collimated THz beam (i.e. without focusing it onto the sample under test) to mimic the plane wave illumination. The THz beam was linearly polarized in horizontal direction, having a beam width at half maximum ~16 mm (see also [33]) that suited well to measuring 3''-samples both at normal and oblique incidence (with θ at least up to 40°). The spectral resolution of the BWO spectrometer in our experiments was around 50 MHz.

3. Results and discussion

3.1. Symmetric spiral disks

In the beginning of our study, we searched for optimal design of spiral disks having narrow-band resonances in the region of 0.2–0.5 THz to allow testing of the fabricated structures with the BWO spectrometer. Under normal illumination of distantly spaced ($p = 768$ μm) spiral disks, the azimuthal symmetry of the disk enables excitation of only dipole LSPR modes [18]. To produce higher order localized "dark" modes (electric or magnetic [21]), we propose to break the symmetry by placing a C-shape resonator near the disk (see Figure 1(c)). The C-resonator exhibits a "bright" mode resonance, which excites the nearby dark spectral modes of the disk. We fixed the resonator radius at $R_C = 204$ μm, while the resonator arch angle α was a variable parameter. Figure 2 shows the calculated transmittance spectra of spiral disks with different α for normal illumination ($\theta = 0°$) by an X-polarized EM wave. Starting from $\alpha = 90°$, the multipole resonances are well excited. With increasing α, the resonances move towards the lower frequencies due to decrease in the bright mode frequency of the C-resonator. For the following simulations we selected $\alpha = 90°$, at which there are several narrowband resonances in the region of 0.2–0.5 THz (see the highlighted region in Figure 2). Another way to excite multipole resonances with a high Q-factor is oblique illumination of the structure, which also breaks the excitation symmetry [20, 34]. The TM-transmittance spectra of distantly spaced spiral disks with a 90°-C-resonator at oblique incidence with $\theta = 0$, 20°, and 40° simulated for two orthogonal orientations ($\varphi = 0$ and $\varphi = 90°$) are plotted in Figure 3(a). Analysis shows that the bright mode of the C-resonator in the vicinity of frequency ≈0.5 THz (see Figure 2, $\alpha = 90°$) is excited most efficiently when the in-XY-plane projection of the incident $\boldsymbol{E}$-field is parallel to the resonator ($\varphi = 0$: $\boldsymbol{E}_X \neq 0$, $\boldsymbol{E}_Y = 0$); in opposite case ($\varphi = 90°$: $\boldsymbol{E}_X = 0$, $\boldsymbol{E}_Y \neq 0$), the bright mode is not revealed. For both orientations, upon increasing θ, the main resonances shift a little and become

weaker due to decreasing the ***E***-projection on the PMS plane. We may also track new resonances arising above 0.38 THz, whose position depend on the incidence angle and probably originates from hybridized nature of these modes.

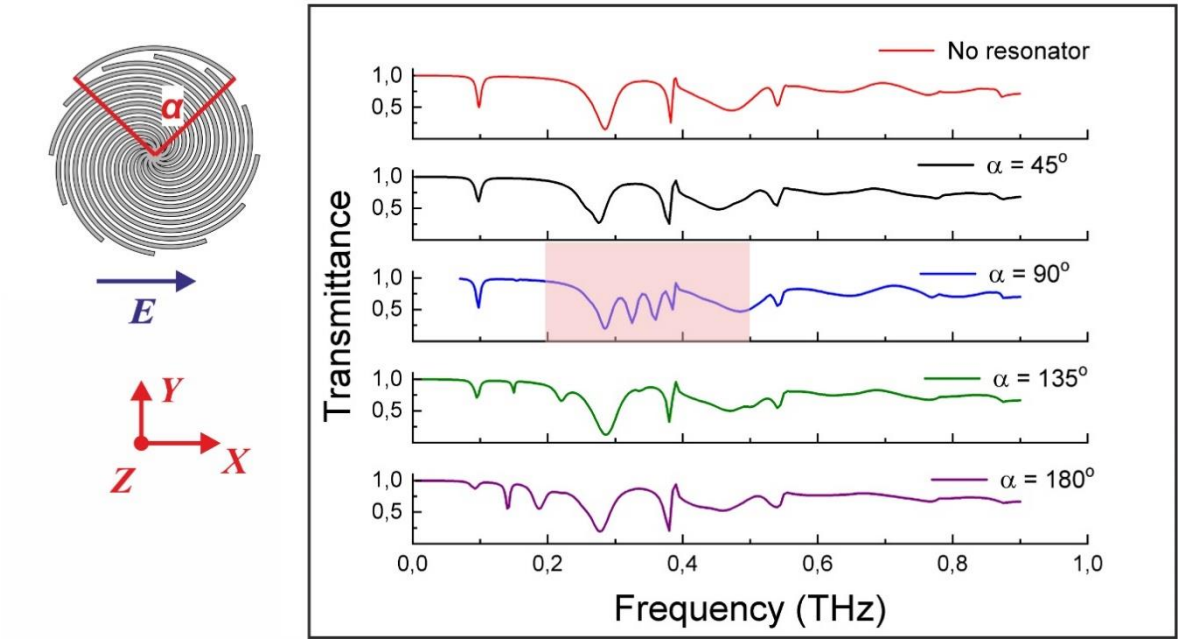

Figure 2. Transmittance spectra of distantly spaced ($p = 768$ μm) spiral disks with different C-resonator angles α. Normal incidence ($\theta = 0°$), $\boldsymbol{E} \parallel X$.

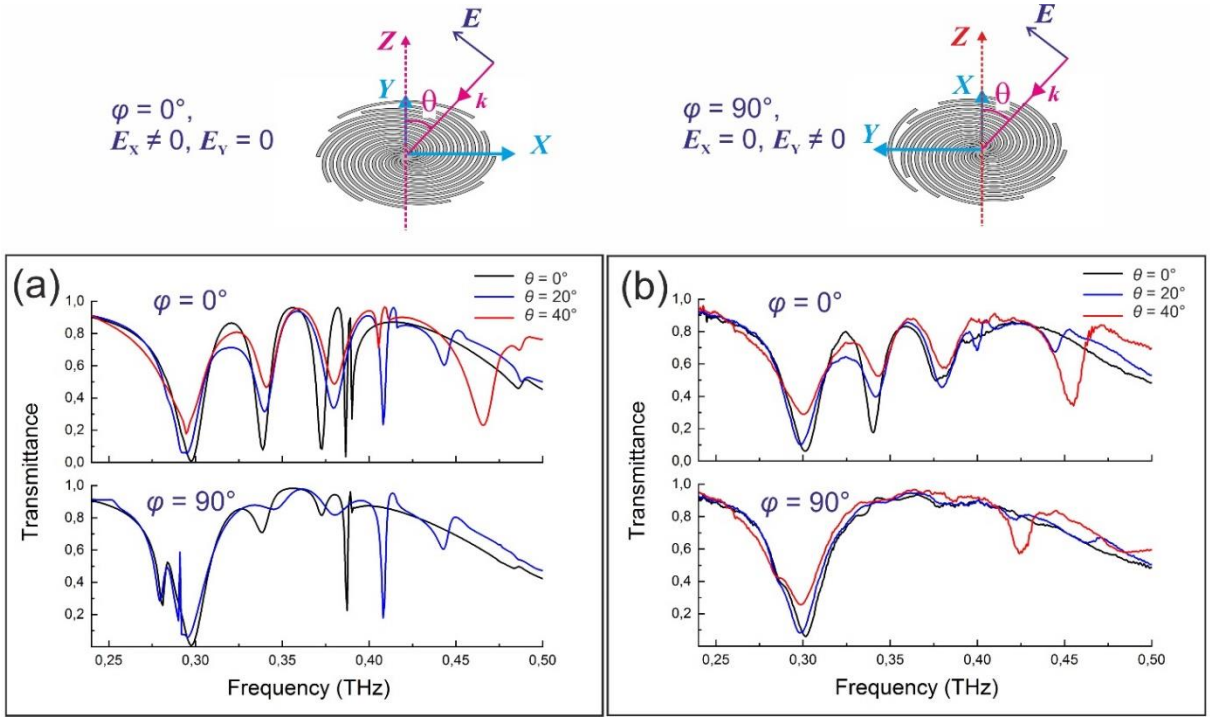

Figure 3. TM-transmittance spectra of distantly spaced spiral disks with 90°-C-resonator under oblique illumination: $\theta = 0$, 20, and 40°: (**a**) simulations; (**b**) experiments. Azimuthal angles $\varphi = 0$ and $\varphi = 90°$ correspond to zero projections of the incident ***E***-field on Y and X axes, respectively.

The experimentally measured TM-transmission spectra of the distantly spaced spiral disks with a 90°-C-resonator patterned on the 15-μm-PP substrate are shown in Figure 3(b). Reasonable mutual agreement is demonstrated between the experimental and simulated data. There are some

discrepancies in the spectral region near 0.38 THz. In simulations, there are two narrowband resonances which are degraded in the experiment. We attribute these differences to the higher THz absorption in real metal-dielectric structures and slight technological spread in the dimensions of the PMS micro-pattern upon its lithographic fabrication.

To characterize the sensing performance of the fabricated metasurfaces, we covered the metallized face of the samples with thin layers of photoresist used as the analyte. The analyte thicknesses after deposition: d = 0.3, 1, 5, and 10 μm (from $2 \cdot 10^{-4}\lambda$ to $7 \cdot 10^{-3}\lambda$). Depositing thicker layers was not feasible due to insufficient viscosity of the employed photoresist. The transmittance spectra of the samples measured with the BWO spectrometer are shown in Figure 4(b). The simulated spectra (see Figure 4(a)) are in good accordance with the experiments. With increasing d, all the resonances are gradually shifted towards lower frequencies. We evaluated the resonance shifts Δf (GHz) from the spectra at 0.297, 0.339, and 0.373 THz as a function of the photoresist thickness d (see Figure 5(a)). The experimental and simulated results are in qualitative agreement. Additional simulations for larger thicknesses showed that Δf tends to saturation at $d > 50$ μm, at which the sensor is insensitive to thickening the photoresist layer.

According to [16], the frequency sensitivity of the sensor is defined as the ratio of the resonance frequency variation to the product of the analyte thickness and refractive index n_a: $S = \Delta f/(d \cdot n_a)$, with the units of GHz·[RIU·mm]$^{-1}$. The dependencies $S(d)$ plotted in Figure 5(b) are almost consistent with each other, except for d = 0.3 μm at which the experimental value S is larger than the simulated one. The reason for this discrepancy presumably lies in a deviation of the real thickness (averaged over a THz-illuminated area) of the photoresist layer deposited on a flexible 15-μm-PP substrate of our PMS sensor.

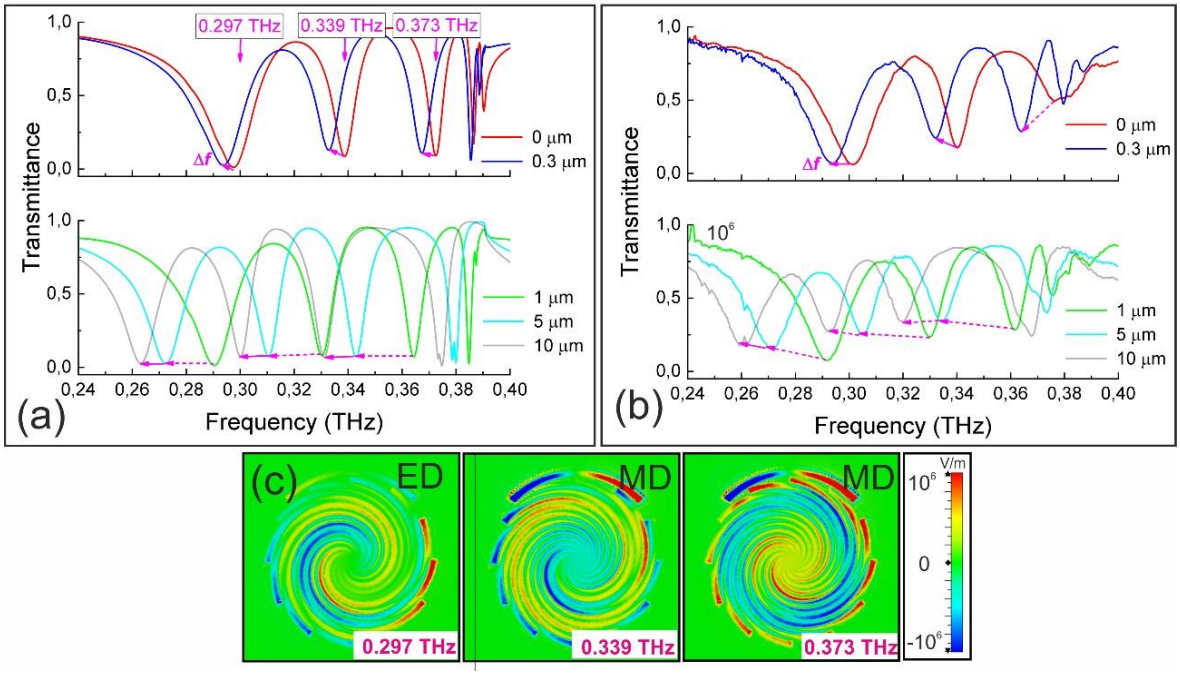

Figure 4. Transmittance spectra of distantly spaced (p = 768 μm) spiral disks with 90°-C-resonator and photoresist coatings of different thicknesses: (**a**) numerical simulations; (**b**) experiments; (**c**) Ez-field distributions at resonances (0.297 THz – natural electric dipole mode (ED), 0.339 THz and 0.373 THz – magnetic dipoles (MDs)). Normal incidence (θ = 0°), $\boldsymbol{E} \parallel X$.

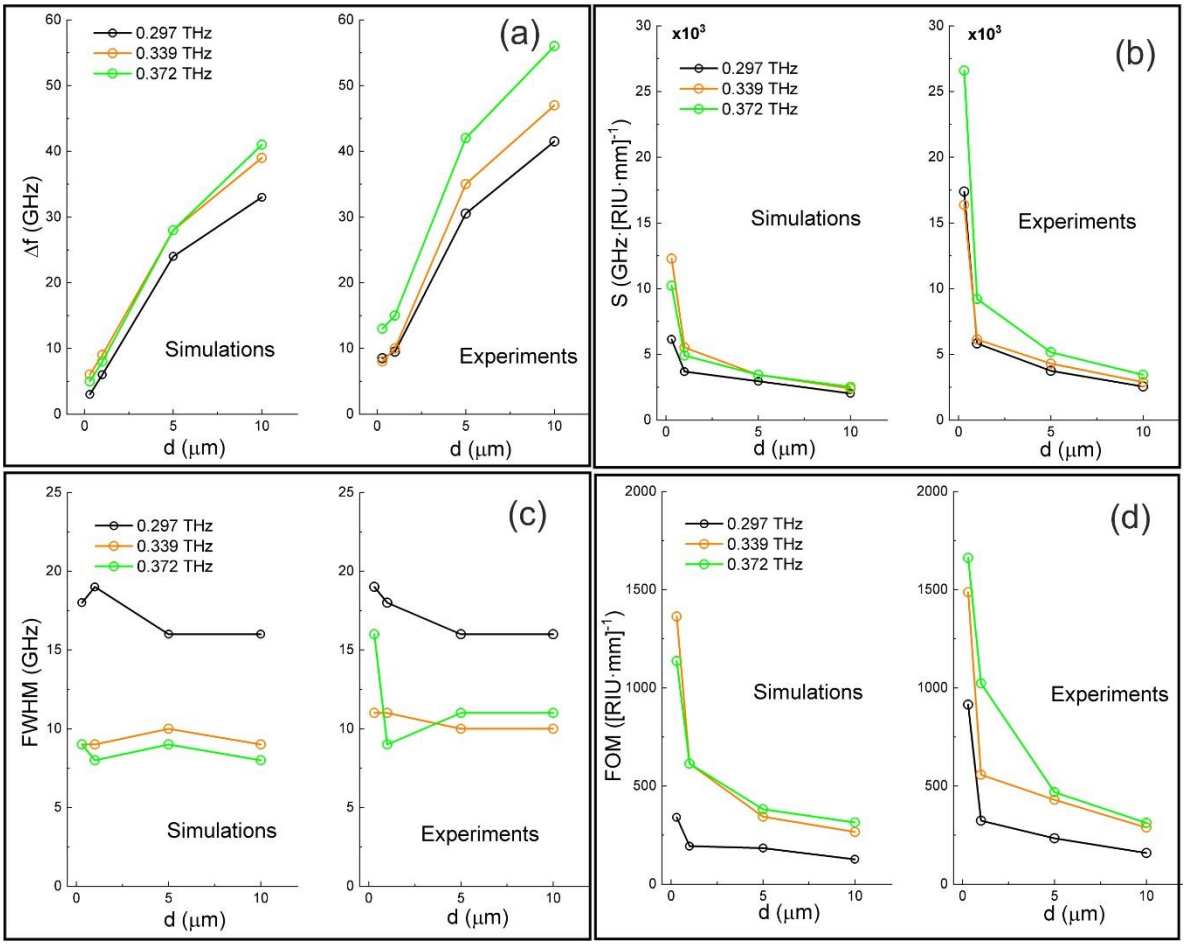

Figure 5. Sensor parameters for distantly spaced ($p = 768$ μm) spiral disks with 90°-C-resonator, evaluated from transmittance spectra in Figure 4: (**a**) frequency shifts Δf of resonances at 0.297, 0.339, and 0.372 THz vs. photoresist thicknesses d (left – simulations, right - experiments); (**b**) sensitivity S vs. d; (**c**) *FWHM* vs. d; (d) *FOM* vs. d.

In sensing applications, the full width at the half minimum (*FWHM*) in the units of frequency is another important characteristic related with the *Q*-factor of the resonance. The *FWHM* versus d is plotted in Figure 5(c). It is worth noticing that the resonance at 0.297 THz has about two times larger *FWHM* as compared to the other two resonances. This effect is explained by their different nature: the mode excited at 0.297 THz is electric-dipole, while the modes at 0.339 THz and 0.373 THz are magnetic-dipole, as illustrated in Figure 4(c) by *Ez*-field distributions simulated at the resonant frequencies at a distance of 2 μm from the metallized layer. According to [22], magnetic modes potentially have higher *Q*-factors than electric ones.

In many cases, the sensitivity alone is not enough to determine the sensor quality. It is clear that to minimize the overlapping between the detection thresholds upon shifting the resonance, resonances with narrower bandwidth can be distinguished better in experiment. From this viewpoint, it is preferable to use sensors with higher values of the figure of merit (*FOM*), which is defined as the ratio $FOM = S / FWHM$, with the units of $[\text{RIU}\cdot\text{mm}]^{-1}$. The calculated graphs of the *FOM* as a function of d depicted in Figure 5(d) show that magnetic resonances are more sensitive than electric ones, especially for very thin analyte layers. The highest *FOM* is attained at $d = 0.3$ μm: $FOM \approx 1670$ $[\text{RIU}\cdot\text{mm}]^{-1}$.

Measurements under oblique illumination of the samples demonstrated that the main resonances (see Figure 3) have the same sensitivity and *FOM* to the analyte as at normal incidence.

3.1. Asymmetric spiral disks with shifted center

Another way to produce high order resonances is to break symmetry of the disk by shifting its center at some value δ*r* (see Figure 1(d)). The δ*r* magnitude affects the number and frequencies of the dark modes. For the new design we took spiral disks with δ*r* = 35 μm, at which multiple resonances are excited in the spectral region of interest 0.2–0.5 THz, and arranged them in the array with higher density packing (*p* = 408 μm). The advantage of densely packed structures lies in red-shifting the LSPRs relative to the diffraction lobes onset point that improves angular stability of resonances [35]. Furthermore, in case of closely spaced disks, new strong plasmon modes can be excited due to hybridizing the EM fields of nearby disks [19, 36]. The results of simulating the transmittance spectra for closely spaced spiral disks with a 135⁰-C-resonator and δ*r* = 35 μm covered with photoresist films of different thicknesses are shown in Figure 6(a).

For clarity, the graphs in Figure 6 are plotted in a reduced spectral region of 0.36–0.48 THz. There are many narrow resonances, which are red-shifted when increasing the photoresist thickness (the shifts are indicated by arrows). The experimental results of the fabricated samples with the same parameters are presented in Figure 6(b). As compared with simulations, there is only one distinct wideband resonance at 0.438 THz in the spectral range considered; other narrow resonances are broadened and disappeared due overlapping with adjacent resonances. The *Ez*-field distribution of two nearby disks at 0.438 THz (Figure 6(c)) presumably corresponds to an electric sextupole hybrid mode. The *FWHM*(*d*) values plotted in Figure 7(c) are approximately the same as for the distantly spaced disks without shifted centers (see Figure 5 (c)), while Δ*f*(*d*) and *S*(*d*) (Figure 7(a,b)) are significantly larger. The greater sensitivity can be explained by the high-density arrangement of the disks, which enhances EM field localization near the PMS. The larger sensitivity yields the greater *FOM*. The highest *FOM* ≈ 2950 [RIU·mm]$^{-1}$ is reached at the smallest analyte thickness (*d* = 0.3 μm) that is ≈ 77 % bigger than in case of distantly spaced disks. This result is comparable with the best *FOM* value (3450 [RIU·mm]$^{-1}$) obtained at the same analyte thickness for a labyrinth metasurface absorber implemented with a similar fabrication techniques [16,35].

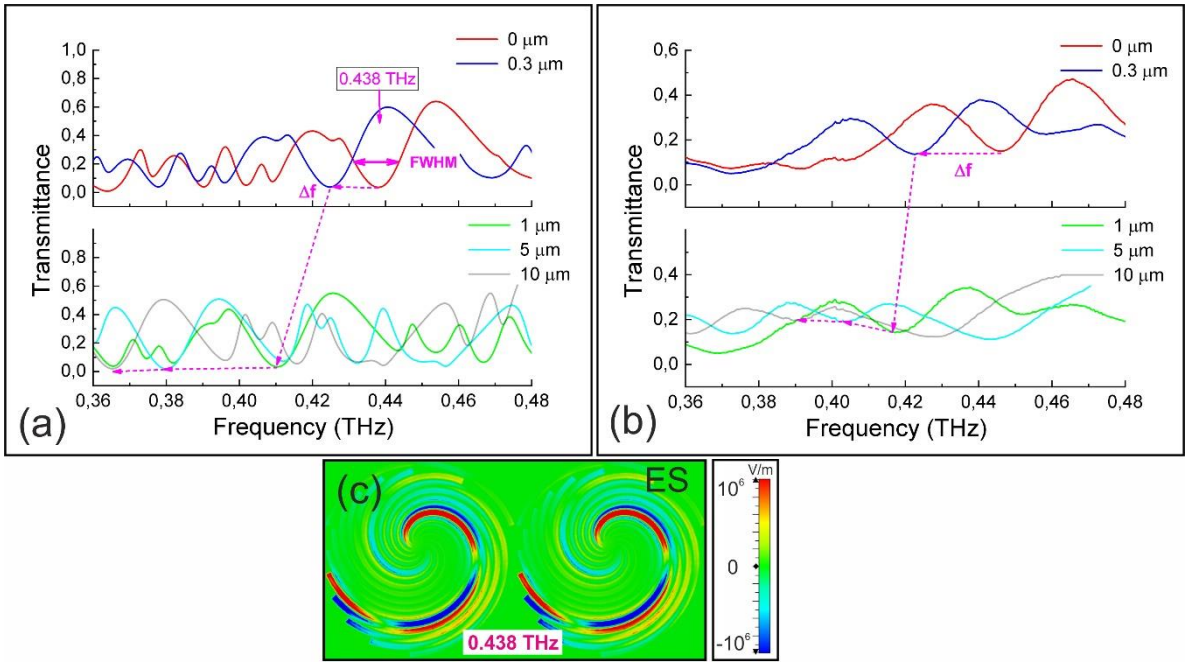

Figure 6. Transmittance spectra of closely spaced (*p* = 408 μm) spiral disks with center shifted at δ*r* = 35 μm covered by photoresist films of different thicknesses: (**a**) numerical simulations; (**b**) experiments; (**c**) *Ez*-field distribution at resonance (0.438 THz). Normal incidence (*θ* = 0°), ***E*** || *X*.

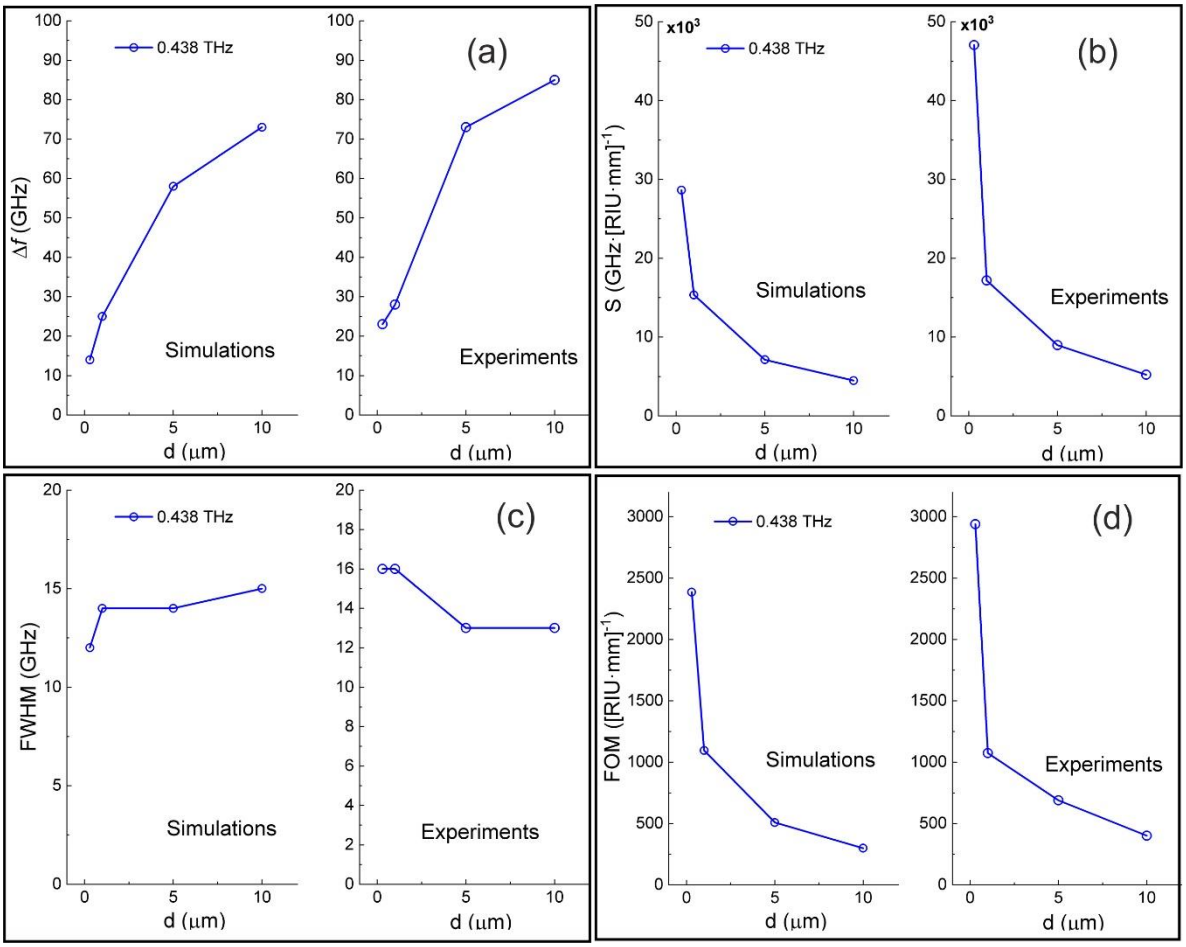

Figure 7. Sensor parameters for closely spaced ($p = 768$ μm) spiral disks with center shifted by $\delta r = 35$ μm, evaluated from transmittance spectra in Figure 7: (**a**) frequency shift Δf of resonance at 0.438 THz vs. photoresist thicknesses d (left: simulations, right: experiments); (**b**) sensitivity S vs. d; (**c**) *FWHM* vs. d; (d) *FOM* vs. d.

5. Conclusions

In summary, we demonstrated high sensing performance of metasurfaces consisting of spiral metallic disks patterned on thin PP substrates, which operate in the low-frequency region of the THz range (0.2-0.5 THz). High Q-factor localized surface plasmon dark modes were excited by placing a C-shaped resonator near the disk. Metasurfaces with optimal design were fabricated by the photolithographic technique and tested with a sub-terahertz CW BWO spectrometer. The experimental transmittance showed good agreement with simulations. The resonance frequency shifts Δf arising from very thin ($d \approx 10^{-4}\,\lambda$) photoresist coatings increases with d, while approaching a constant at $d = 50$ μm. Dark magnetic modes excited on symmetric spiral disks with 90^0-C-resonators demonstrated very high *FOM* values, especially for the smallest thicknesses (1670 $[\text{RIU}\cdot\text{mm}]^{-1}$ at $d = 0.3$ μm) due to a narrow resonance width. The hybrid high order mode resonances of asymmetrical densely packed spiral disks (with a shift of the disk center) showed about two times larger *FOMs* (up to 2950 $[\text{RIU}\cdot\text{mm}]^{-1}$) versus symmetrical spirals, that is comparable with the best *FOM* values obtained for alternative metasurfaces with densely packed unit cells fabricated with a similar technique. The attained results allow us to highlight the spiral disks design as promising for bio-sensing applications in the THz range.

Author Contributions: Conceptualization, V.V.G.; methodology, V.V.G. and S.A.K.; software, R.R.H. and S.A.K..; validation, V.V.G., R.R.H. and P.A.L.; formal analysis, V.V.G. and S.A.K.; investigation, V.V.G. and R.R.H.; resources, S.A.K.; data curation, V.V.G.; writing—original draft preparation, V.V.G.; writing—review and editing, S.A.K.; visualization, V.V.G. and R.R.H.; supervision, V.V.G.; project administration, V.V.G.; funding acquisition, V.V.G. All authors have read and agreed to the published version of the manuscript.

Funding: This research was funded by the Russian Science Foundation, grant number 18-72-00112.

Acknowledgments: The work was done using the infrastructure of the Shared Research Facility "Siberian Synchrotron and Terahertz Radiation Centre" of BINP SB RAS and the Shared Equipment Center CKP "VTAN" (ATRC) of the NSU Physics Department. Authors thanks A. V. Gelfand and N. I. Fedorinina for the sample preparation.

Conflicts of Interest: The authors declare no conflict of interest. The funders had no role in the design of the study; in the collection, analyses, or interpretation of data; in the writing of the manuscript, or in the decision to publish the results.

References

1. Maier, S. A. *Plasmonics: Fundamentals and Applications*, Springer Verlag: New York, 2007.
2. Anker, J. N.; Hall, W. P.; Lyandres, O.; Shah, N. C.; Zhao, J.; Van Duyne, R. P. Biosensing with plasmonic nanosensors. *Nature Materials* **2008**, *7*, 442–453.
3. Stiles, P. L.; Dieringer, J. A.; Shah, N. C.; Van Duyne, R. P. Surface-enhanced Raman spectroscopy. *Annual Review of Anal. Chem.* **2008**, *1*, 601–626.
4. Lakowicz, J. R.; Ray, K.; Chowdhury, M.; Szmacinski, H.; Fu, Yi; Zhang, J.; Nowaczyk, K. Plasmon-controlled fluorescence: a new paradigm in fluorescence spectroscopy. *Analyst* **2008**, *133*, 1308–1346.
5. Valev, V. K.; Silhanek, A. V.; Verellen, N.; Gillijns, W.; Van Dorpe, P.; Aktsipetrov, O. A.; Vandenbosch, G. A.; Moshchalkov, V. V.; Verbiest, T. Asymmetric optical second-harmonic generation from chiral G-shaped gold nanostructures. *Phys. Rev. Lett.* **2010**, *104*, 127401.
6. Atwater, H. A.; Polman, A. Plasmonics for improved photovoltaic devices. *Nature Materials* **2010**, *9*, 205–213.
7. Tian, Y.; Tatsuma, T. J. Mechanisms and applications of plasmon-induced charge separation at TiO2 films loaded with gold nanoparticles. *J. Am. Chem. Soc.* **2005**, *127*, 7632–7637.
8. Son, J.-H., Ed. *Terahertz Biomedical Science and Technology*, CRC Press; Boca Raton, Florida, 2014.
9. Peiponen, K.-E., Zeitler, J. A., Kuwata-Gonokami, M., Eds. *Terahertz spectroscopy and imaging. Springer series in optical sciences*, vol.171, Berlin Heidelberg: Springer-Verlag; 2013.
10. Lee, Y.-S. *Principles of terahertz science and technology*, Springer-Verlag: New York, 2009.
11. Ordal, M. A.; Bell, R. J.; Alexander, R. W.; Long L. L.; Querry M. R. Optical properties of fourteen metals in the infrared and far infrared: Al, Co, Cu, Au, Fe, Pb, Ni, Pd, Pt, Ag, Ti, and W. *Applied Optics* **1985**, *24* (24), 4493-4499.
12. Pendry J. B.; Martin-Moreno, L.; Garcia-Vidal, F. J. Mimicking surface plasmons with structured surfaces. *Science* **2004**, *305*, 847-848.
13. Pors, A.; Moreno, E.; Martin-Moreno, L.; Pendry, J. B.; Garcia-Vidal, F. Localized spoof plasmons arise while texturing closed surfaces. *Phys. Rev. Lett.* **2012**, *108*, 223905.
14. Glybovski, S. B., Tretyakov, S. A., Belov P. A., Kivshar, Yu. S., Simovski, C. R. Metasurfaces: from microwaves to visible. *Phys. Reports*. **2016**; *634*, 1–72.
15. Al-Naib, I.; Withayachumnankul, W. Recent progress in terahertz metasurfaces. *J. Infrared, Millimeter, and Terahertz Waves* **2017** *38*, 1067–1084.
16. Beruete, M.; Jáuregui-López, I. Terahertz sensing based on metasurfaces. *Adv. Optical Mater.* **2020**, *8*, 1900721.
17. Liao, Z.; Shen, X.; Pan, B. C.; Zhao, J.; Luo, Yu; Cui, Tie Jun. Combined system for efficient excitation and capture of LSP resonances and flexible control of SPP transmissions. *ACS Photonics* **2015**, *2 (6)*, 738-743.
18. Chen, L.; Wei, Y. M., Zang, X. F.; Zhu, Y. M.; Zhuang, S. L. Excitation of dark multipolar plasmonic resonances at terahertz frequencies. *Sci. Rep.* **2016**, *6*, 1-11.
19. Bulgakova V.; Gerasimov, V.; Lemzyakov, A.; Milekhin, I. A. Infrared localized surface plasmon resonances on subwavelength corrugated metal disks. Proceedings of 43-th International conference IRMMW-THz, Nagoya, Japan, 9-14 Sept., IEEE, 2018.
20. Gerasimov, V. V.; Kuznetsov, S. A.; Lemzyakov, A. G.; Hafizov, R. R. Multipole terahertz localized plasmon resonances on spiral structures. Proceedings of 44-th International conference IRMMW-THz, France, Paris, 1-6 Sept., IEEE, 2019.
21. Huidobro, P. A.; Shen, X.; Cuerda, J.; Moreno, E.; Martin-Moreno, L.; Garcia-Vidal, F. J.; Cui, T. J.; Pendry, J. B. Magnetic localized surface plasmons. *Phys. Rev. X* **2014,** *4*, 021003.

22. Gao, Z.; Wu, L.; Gao, F.; Luo, Y.; Zhang, B. Spoof Plasmonics: from metamaterial concept to topological description. *Adv. Mater.* **2018**, *30*, 1706683.
23. Liao, Z.; Fernández-Domínguez, A. I.; Zhang, J.; Maier, S. A.; Cui, T. J.; Luo, Yu. Homogenous metamaterial description of localized spoof plasmons in spiral geometries. *ACS Photonics* **2016**, *3*, 1768−1775.
24. Liao, Z.; Liu, S.; Ma, H. F.; Li, C.; Cui, J.; Cui, T. J. Electromagnetically induced transparency metamaterial based on spoof localized surface plasmons at terahertz frequencies. *Scientific Reports* **2016**, *6*, 27596.
25. Kuznetsov, S. A.; Paulish, A. G.; Navarro-Cía, M.; Arzhannikov, A. V. Selective pyroelectric detection of millimetre waves using ultra-thin metasurface absorbers. *Sci. Rep.* **2016**, *6*, 21079.
26. Navarro-Cia, M.; Kuznetsov, S. A.; Aznabet, M.; Beruete, M.; Falcone, F.; Ayza, M. S. Route for bulk millimeter wave and terahertz metamaterial design. *IEEE J. Quantum Electron* **2011**, 47, 375–385.
27. Aznabet, M.; Navarro-Cía, M.; Kuznetsov, S. A.; Gelfand, A. V.; Fedorinina, N. I.; Goncharov, Y. G.; Beruete, M.; Mrabet, O. El; Sorolla, M. Polypropylene-substrate-based SRR- And CSRR-metasurfaces for submillimeter waves. *Opt. Express* **2008**, *16*, 18312–18319.
28. Kuznetsov, S.A.; Arzhannikov, A.V.; Kubarev, V. V.; Kalinin, P.V.; Sorolla, M.; Navarro-Cía, M.; Aznabet, M.; Beruete, M.; Falcone, F.; Goncharov, Y.G.; Gorshunov, B.P.; Gelfand, A. V.; Fedorinina, N.I. Development and characterization of quasi-optical mesh filters and metastructures for subterahertz and terahertz applications. *Key Eng. Mater.* **2010**, *437*, 276–280.
29. ALLRESIST GmbH. https://www.allresist.com
30. Jauregui-López, I.; Rodriguez-Ulibarri, P.; Kuznetsov, S. A.; Nikolaev, N. A.; Beruete, M. THz sensing with anomalous extraordinary optical transmission hole arrays. *Sensors* **2018**, *18*, 3848.
31. Kozlov, G.; Volkov, A. Coherent source submillimeter wave spectroscopy. In *Millimeter and Submillimeter Wave Spectroscopy of Solids. Topics in Applied Physics*, Grüner, G., Ed.; Springer-Verlag Berlin, Heidelberg, 1998, Vol. 74, pp. 51 –109.
32. Sayanskiy, A.; Kuznetsov, S. A.; Tanygina, D. S.; Risco, J. P.; Glybovski, S.; Baena, J. D. Frequency controllable polarization rotation of THz waves with an SCMS. *IEEE Transactions on Antennas and Propagation* **2019**, *68(3)*, 1491-1502.
33. Kuznetsov, S. A., Paulish; A. G.; Gelfand, A. V.; Lazorskiy, P. A.; Fedorinin, V. N. Bolometric THz-to-IR converter for terahertz imaging. *Appl. Phys. Lett.* **2011**, *99*, 023501.
34. Rodríguez-Ulibarri, P.; Kuznetsov, S. A.; Beruete M. Wide angle terahertz sensing with a cross-dipole frequency selective surface. *Appl. Phys. Lett.* **2016**, *108*, 111104
35. Jáuregui-López, I.; Rodríguez-Ulibarri, P.; Urrutia, A.; Kuznetsov, S.A.; Beruete, M. Labyrinth metasurface absorber for ultra-high-sensitivity terahertz thin film sensing. *Phys. Status Solidi.* **2018**, *12*, 1800375.
36. Zhang, J.; Liao, Z.; Luo, Yu; Shen, X.; Maier, S. A.; Cui, T. J. Spoof plasmon hybridization. *Laser & Photonics* **2017**, *11(1)*, 1600191.